RESEARCH

Depositional dynamics of the Bengal Fan since the Late Miocene: discrimination of skinfriction shear stresses of hemipelagic vs. turbiditic deposition

M. Kawsar[1,2] · M. C. Manoj[1,2] · M. E. Weber[3]

Abstract

The Bengal Fan covers the entire floor of the Bay of Bengal (BoB) and has accumulated erosional material from the Himalayas since the Early Eocene. The fan architecture is constructed by turbidity current deposits via channel levee systems during active fan progradation and hemipelagic sedimentation during periods of local fan inactivity. In the present study, we document the fan development, sedimentation history, and depositional processes in the lower Bengal Fan and present a site-to-site comparison of stratigraphy and channel migration since the Late Tortonian (ca. 7.5 Ma) from sedimentological and physical property records at Site U1451 of IODP Expedition 354 to 8°N in the lower Bengal Fan. Fine sediment (Sortable Silt, SS) textural and sorting records are used to reconstruct the current skinfriction shear stress in the Benthic Boundary Layer (BBL) of the BoB. Also, a distinction in shear stress environment between turbidity dominated active fan and background hemipelagic fan growth is presented. A criterion is set in the following paper to validate the use of SS records in hemipelagic deposits in the BoB to decipher the shear stress regimes of depositing flows on the basis of sand weight percentage and mean SS sizes ($\overline{SS}$) variation. This study will enhance our understanding of the Bengal Fan deposition dynamics and fan development with the reconstructed shear stress regimes associated with various depositing flows (turbidity current and/or deep water circulation). It will provide a strong base to model fan internal processes and material flux to the BoB.

Introduction

The Bengal Fan is the largest submarine fan accommodating a huge stack of continental erosional materials since the Indo-Tibet-Burma collision in the early Miocene at 22 Ma (Alam et al. 2003). It holds the least ambiguous and uninterrupted records of tectonic-climatic evolution through Himalayan uplift and erosion since the major collisional events (Derry and France-Lanord 1997; Zhisheng et al. 2001; Curray et al. 2003). An enormous volume of sediment laden discharge from terrestrial rivers is delivered to the passive continental shelves from where submarine canyons direct the sediment plumes to the deep abyss of the Bay of Bengal (BoB), bypassing the continental slopes. The fan architecture is built by turbidity current deposition delivered via channel levee systems during active fan progradation and hemipelagic sedimentation during periods of local fan inactivity hence making it a mixed hemipelagic-turbidite dominated fan (France-Lanord et al. 2016; Weber and Reilly 2018). Bengal Fan has been extensively studied for the morphology, stratigraphy, and processes (e.g., Curray and Moore 1971; Curray et al. 2003). Sediment transportation mechanism, fan internal cycles, and sediment physical properties in response to the external forcing are well established in the literature (Weber et al. 1997a; 1997b; 2003). Seismic observations were conducted during several deep sea drillings and cruise excursions in the BoB (e.g., DSDP Leg 22, ODP Leg 116, R V Sonne

✉ M. C. Manoj
manoj_mc@bsip.res.in

M. Kawsar
masudkawsar@bsip.res.in

M. E. Weber
mike.weber@uni-bonn.de

[1] Birbal Sahni Institute of Palaeosciences, Uttar Pradesh, Lucknow 226007, India

[2] Academy of Scientific and Innovative Research (AcSIR), Ghaziabad 201002, India

[3] Department of Geochemistry and Petrology, Institute for Geosciences, University of Bonn, 53115 Bonn, Germany

125), and detailed high resolution seismic stratigraphic records are acquired along several seismic profiles in the upper, middle, and lower Bengal Fan (Spieß et al. 1998; Curray et al. 2003; Schwenk et al. 2003; 2005; Schwenk and Spieß, 2009).

IODP Expedition 354 drilled seven sites at 8° north in the lower Bengal Fan (Fig. 1) along the seismic profile GeoB97-020/027 (Fig. 1a) of the R V Sonne cruise 125 (Spieß et al., 1998) and across the central axis of the fan (France-Lanord et al. 2016). One deep Site U1451 (8°0.42′N, 88°44.50′E at 3607.3 m water depth) to 1200 m below seafloor (mbsf) recovered a complete sequence of fan deposits, in particular, to reach the pre-fan section. High-resolution multichannel seismic records (Bergmann et al. 2020) reconstructed seismic facies in all expedition 354 sites and mapped buried channel levees systems across the lower Bengal Fan. Fan progradation is comprehensively described in terms of Subfan (A, B, C, and D) originally introduced by Curray et al. (2003). Subfan signifies active fan deposition connected to a single channel levee system at a time. Based on seismic investigations, Bengal Fan deposition has been very complex due to frequent avulsion of channel levees in the upper fan and formation of new channel levees and successive autocyclic migration of depocenter across the central axis of the fan, which changed the sediment focusing to the east and west of 85°

Ridge in the BoB (Curray et al. 2003; Schwenk and Spieß, 2009; Bergmann et al. 2020). A migrating depocenter also implies not all of the fans received direct sediment input from the active channel levees and part of the fan remains distal to the active fan deposition. Intense channel incision and levee deposition have been the dominant sedimentation process modulated by turbidity currents in the active fan, whereas in the most distal part of the fan, hemipelagic sediments accumulated in the background. There are variable rates of sediment accumulation across the fan margins. Turbiditic intervention is not inherent to the hemipelagic deposits of the fan and sediment accumulation is more likely to be administrated by local deep water flow regimes. Regionally extensive hemipelagic layers, for instance, MPHL (Middle Pleistocene Hemipelagic layer) and LPHL (Late Pleistocene hemipelagic layer) recovered from the Expedition 354 sites have been investigated to reconstruct monsoonal variability from physical properties of deposited sediments in response to the allocyclic (e.g., solar insolation) controls. These layers clearly responded to allocyclic controls such as orbital variability of incoming solar radiation and the long-term Pleistocene climate evolution (Kawsar et al. 2022; Weber et al. 2018; Weber and Reilly 2018) rather than the autocyclic processes that dominate the fan sedimentation in between these times. Also, recent paleoceanographic reconstruction in one of
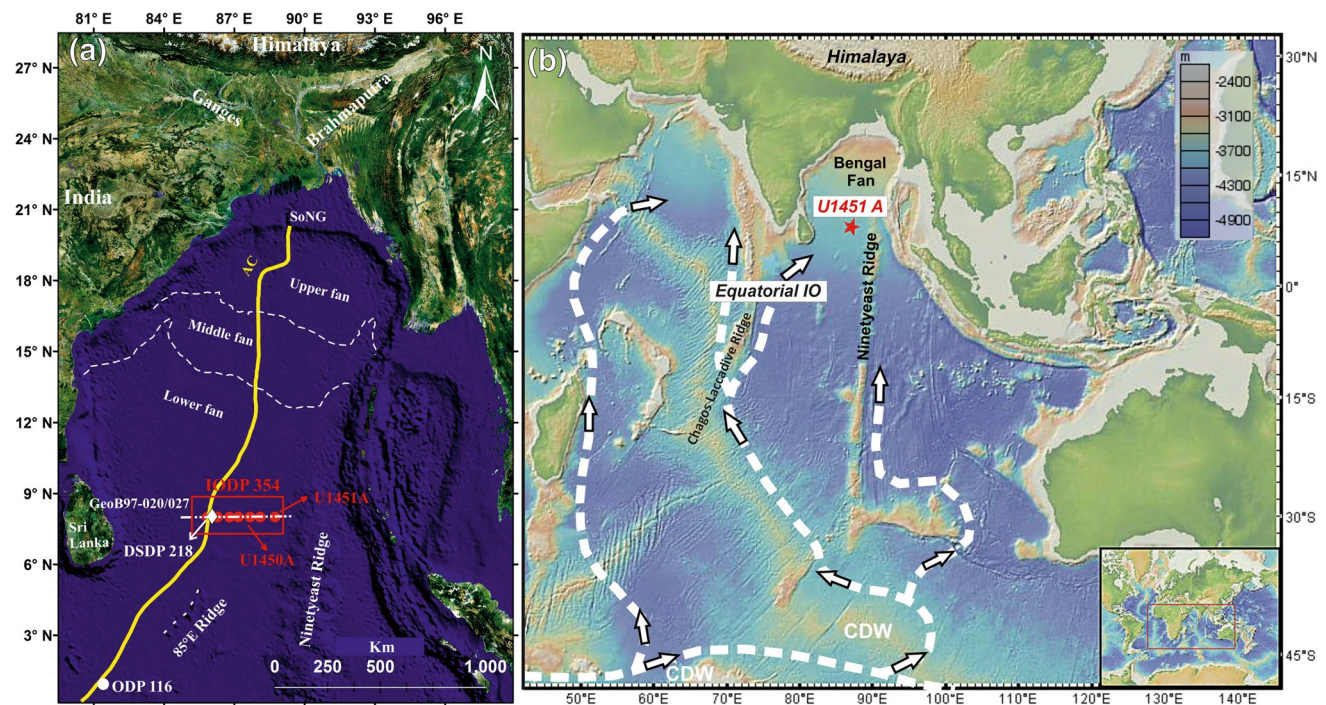

Fig. 1 a Map of Bengal Fan and core locations. SoNG, Swatch of No Ground; AC, Active Channel modified after Weber and Reilly (2018). Water depth in upper fan (<2500 m), middle fan (2500 to 3500 m) and lower fan (>3500 m). Dash-dot line represents the seismic section GeoB97-020/027 (Spieß et al., 1998) along which DSDP Site 218 and IODP Expedition 354 sites (red) were drilled. **b** Flow paths of Circumpolar Deep Water (CDW) and important bathymetric features in the Indian Ocean including site U1451

the regionally extensive hemipelagic layer, i.e., the LPHL in the hole U1452C of IODP expedition 354 shows that the sorting of fine sediments (particularly the silt sized particles) is governed by the intensity of the Atlantic Meridional Overturning Circulation (AMOC) and variable fluxes of deep north Atlantic as well as Southern Ocean sourced deep and bottom waters (i.e., ancient NADW and AABW) during the glacial-interglacial cycles of the last 200 ka (Kawsar et al. 2022). These fine sediment sorting evidences are concordant with radiogenic Nd isotope ratio based deep water-mass end member reconstruction in the Northern Indian Ocean (e.g., Piotrowski et al. 2009; Lathika et al. 2021) and late Pleistocene paleoceanographic and paleoclimatic changes (details in Kawsar et al. 2022 and the references there in). Hemipelagic layers also provide a very good chronostratigraphic framework in site-to-site comparison of sedimentation and provide excellent age control points (Reilly et al. 2020; Weber et al. 2018).

In the present study, we aim to reconstruct the Bengal Fan sedimentation history beyond the time scale of Subfan A (i.e., 1.9 Ma: Late Gelasian) and present a continuous record of fan development to the easternmost Site (U1451) of IODP Expedition 354 since the Late Tortonian (ca. 7.5 Ma). High-resolution downcore physical property measurements, i.e., Natural Gamma Radiation (NGR) precisely distinguished lithostratigraphic facies changes while the magnetostratigraphic and sediment lightness (*L** values) record provided excellent age control points to set up a robust age model that describe the temporal variation in sedimentation at the hole U1451A and precisely discriminate between the exact timing of channel levee deposition and background hemipelagic sedimentation. These findings add valuable information on the overall fan development by comparing major lithologies and sediment textural parameters at the Sites U1450 (along the central axis of the fan) and U1451 and possible depocenter migration as well as variable fan deposition across the lower Bengal Fan. This study uses yet another thick hemipelagic layer deposited during ~2.4 to ~5.7 Ma at Site U1451 to present a numerical model that approximates the shear stress regime of background deposition and distinguishes the two different fluid shear environments (namely, turbid and background) in the Benthic Boundary Layer (BBL) of BoB. Sortable Silt (SS) size distribution and sorting evidence have been utilized in this numerical approach to reconstruct current skinfriction shear stress operated in the BBL delivered by local deep water masses via approximation of sediment threshold of motion. Fine sediment record particularly the non-cohesive SS (10 to 63 μm) mean grain size ($\overline{SS}$) is noted to be a relative flow intensity indicator of deep and bottom water masses (McCave et al. 1995; McCave 2008). SS has been used as a proxy to reconstruct the paleocurrent intensity from different parts of the global deep ocean (e.g.,

Bianchi and McCave 1999; Hall et al. 2004; Praetorius et al. 2008; Roberts et al. 2012; Jessen and Rasmussen 2015; Thornalley et al. 2019; Li et al. 2019). The sediment threshold of motion implies the critical condition to initiate incipient motion in sediment grains. It arises from the balance of stabilizing forces due to the submerged weight of the sediment grain to the hydrodynamic drag forces exerted by the moving fluid. The balance of these forces yields the threshold criterion or the dimensionless bed shear stress (θ_{cr}), initially used by Shields (1936) in the Shields curve (Fig. 2). The numerical approximation of the threshold is given by the threshold bed shear stress ($\mathcal{T}_{cr}$) which is the amount of shear stress necessary to move the sediment grain. It is obtained from the solution of the modified Shields curve given by Soulsby and Whitehouse (1997). On the other hand, skinfriction shear stress approximates the actual fluid shear stress imparted by the bottom water masses. SS size parameters (e.g., $\overline{SS}$ and SS volume %) in the in the hemipelagic sections of the Site U1451A and their applicability in quantifying the BBL fluid shear stresses is argued in the present study. This study will provide a quantitative measure of the shear stress regime of depositional dynamics and fan development. It will help to demonstrate the fan internal and external processes with numerical figures.

Regional hydrography

Deep and bottom waters that originate in the polar region and travel across the western and central Indian Ocean to the corresponding ocean basin are delivered to both the Arabian Sea and the BoB. In contrast to the BoB, which travels along the central Indian Ocean, deep waters in the western path move as the deep western boundary current northward via the Madagascar-Mascarene Basin and into the Arabian Sea (Fig. 1b). Additionally, the BoB receives deep waters from the West Australian Basin through the eastern Circumpolar Deep Water (CDW) branch that enters the eastern Indian Ocean basins (You 2000; Gordon et al.; 2002; McCave et al.; 2005; Piotrowski et al. 2009). The majority of the high salinity Arabian Sea water influx into the southern BoB at depths between 100 and 300 m can be seen in the trajectory of Argo floats installed in the Arabian Sea (Supplementary Fig. 1a). Earlier studies on the watermass structure in the BoB (e.g., Sastry et al. 1985; Kumar and Li 1996; You 2000) show that the BoB and the northern Indian Ocean seasonally reversed surface and thermocline circulations, which are caused by the Indian monsoon (Sastry et al. 1985; Rao and Murty 1992; Shankar et al. 2002). According to inverse hydrographic modelling based on dissolved Nd and εNd values in the water column along a north–south transect in the
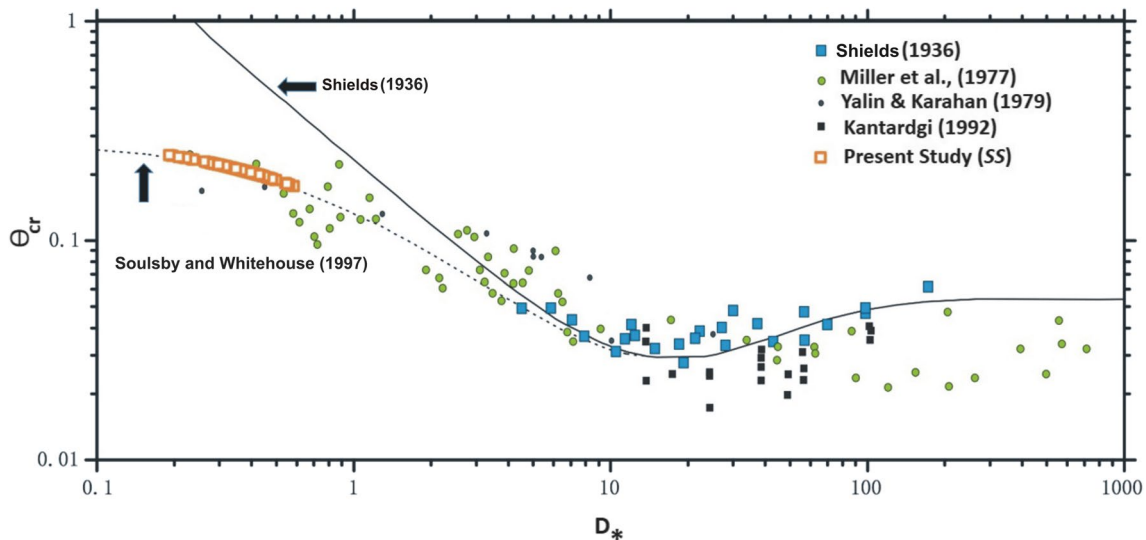
Fig. 2 Threshold curve for currents with non-dimensional axes. Θcr and D* are the Dimensionless bed shear stress (Shields criterion) and the Dimensionless grain diameter. Blue squares (Shields 1936), green circles (Miller et al. 1977), black circles and squares (Yalin and Karahan 1979; Kantardgi, 1992), orange squares (𝒮𝒮 values of present study)

BoB, the BoB Lower Salinity Water (BoBLS) and Indonesian Throughflow Surface Water (IW) dominate the surface layer waters (50 m) in the northern BoB. Arabian Sea High Salinity Water (ASHS), which enters the southern BoB from the Arabian Sea at a depth of 50 to 100 m and moves northward (Sastry et al. 1985) (Supplementary Fig. 1b), lies beneath the surface layer in the southern BoB, which is where this low salinity water is located. The high salinity North Indian Intermediate Water (NIIW), which is a mixture of Red Sea Water (RSW) and Persian Gulf Water (PGW) with ASHS waters, is present at depths of 300–500 m in both the north and south of the BoB (Singh et al. 2012; Goswami et al. 2014). North Indian Deep Water (NIDW) at a depth of around 900 m makes up the water mass in the BoB below the NIIW. Due to the mixing of southward flowing NIIW with Circumpolar Deep Water (CDW), a mixture of Modified North Atlantic Deep Water (MNADW) and Antarctic Bottom Water (AABW), it is believed to have its origins in the Indian Ocean (Wyrtki 1973; Kumar and Li 1996). According to Singh et al. (2012), MNADW dominates deep waters in the BOB at depths of 1700 m and lower, while AABW predominates at depths of 3800 m (Supplementary Fig. 1b). However, NIDW and MNADW in the BoB both occur at shallower depths than their counterparts in the Arabian Sea and the Madagascar basin (e.g., Bertram and Elderfield 1993; Goswami et al. 2014), indicating progressive shoaling of Atlantic-derived waters during their transport from south to north in the Indian Ocean and the BoB.

Methods and material

Sortable silt

Sortable silt grain-size distribution was analyzed within the terrigenous sub-fraction 10 to 63 µm, as defined by McCave et al. (1995). The sediment samples are wet sieved through a 230 mesh (American Society for Testing and Martials, ASTM) separating the sand fraction (˃ 63 µm). Prior to the SS analysis, organic matter was removed from the sieved fine fraction by adding 10% H_2O_2; carbonate was removed by dissolution in 1 M acetic acid solution (48 h at room temperature); biogenic opal was removed by digestion in 2 M sodium carbonate solution (85 °C for 5 h). SS size measurements were undertaken on the residual terrigenous sub-fractions using a Beckman Coulter particle size analyzer and the mean sortable silt grain size (𝒮𝒮) was calculated using the geometric method of moments using GRADISTAT program (Blott and Pye 2001) from the below formula.

$$x_g = \exp\frac{\sum f \text{Inm}_m}{100} \tag{1}$$

Here, x_g is 𝒮𝒮, f is the frequency in percentage, m_m is the middle point of each grain size bins in metric scale (micron, µm). Volume percentage of SS was calculated out of total volume of materials < 63 µm as SS vol% = volume % (10–63 µm)/volume % total fine (< 63 µm). Cohesive volume percentage was calculated

the same viz. cohesive vol% = volume % (< 10 μm)/ volume % total fine (< 63 μm). Sand weight percentage was calculated as (sieved sand weight)/(the weight of samples).

The SS threshold of motion and current skinfriction shear stress

The threshold bed shear stress ($\mathscr{T}_{cr}$) cannot be calculated directly; instead, it is estimated from the threshold criterion expressed by the following equation of dimensionless bed shear stress (θ_{cr}) originally used in the Shields diagram (Fig. 2) by Shields (1936).

$$\theta_{cr} = \frac{\tau_{cr}}{g(\rho_s - \rho)d} \tag{2}$$

Here, $\mathscr{T}_{cr}$ is bed shear stress exerted by the fluid on sediment grains at the threshold of motion, g is the acceleration due to gravity, ρ_s and ρ are the density of the grain, and density of fluid, respectively, and d is the sediment grain diameter. The Shields parameter (θ_{cr}) can be approximated by an algebraic expression given by Soulsby and Whitehouse (1997).

$$\theta_{cr} = \frac{0.30}{1 + 1.2D*} + 0.055\left[1 - \exp^{(-0.020D*)}\right] \tag{3}$$

where D_* is dimensionless grain diameter given by the equation,

$$D* = \left[\frac{g(s-1)}{v^2}\right]^{\frac{1}{3}} d \tag{4}$$

The value of $g = (9.81$ m/s$^2)$, s ($\rho_s / \rho) = 2.52$ given that the value of fluid density (ρ) is taken corresponding to the density of the deep water masses equal to 1050 kg/m^3, and the grain density ($\rho_s = 2650$ kg/m^3) is the density of quartz (McCave et al. 2017), v is the kinematic viscosity of water (1.67×10^{-7} m^2 s^{-1}) at 2 °C (McCave 2008). The measured values of SS size in the core are taken as grain diameter d (in μm). The θ_{cr} is determined from Eq. (2) with the calculated values of D_*. The $\mathscr{T}_{cr}$ was calculated from Eq. (2) using calculated values θ_{cr} and known values of g, ρ_s, ρ, and measured values of d (SS). Figure 2 shows that the data points fall within the proposed asymptote by Soulsby and Whitehouse (1997). The solid line through the data points is the asymptote suggested by Shields, and the dashed line is the modification by Soulsby and Whitehouse (1997) for $D^* < 1$. The later modification allows the threshold calculation for very fine grains (down to silt and clay) and narrows down the overestimation of threshold in that region of the Shields diagram.

Current skinfriction via *estimation of C_{100} and U_{100}*

The current skin-friction shear stress, $\mathscr{T}_{0\,s}$ at 1 mab (meter above the bed), was approximated from the equation $\mathscr{T}_{0\,s} = \rho C_{100} U_{100}{}^2$ via the estimation of drag coefficient (C_d) and boundary layer flow speed (U_g). C_{100} refers to C_d at 1 mab (meter above the bed). C_d is the frictional resistance of the flow and is estimated from examples of experimental and shallow water flows. It is dependent on the bed roughness length Z_0 and the thickness of the flow (water depth) via the equation,

$$C_d = \left[\frac{k}{B + \ln \frac{Z_0}{h}}\right]^2 \tag{5}$$

where k is Von Karman constant (0.4), B is 1, and h was taken 1 mab. The roughness length Z_0 is a certain height above the bed where the flow is retarded due to frictional resistance and is a function of the viscosity of the water, the current speed and the dimensions of the physical roughness of the bed. The value of Z_0 was taken as typical of mud (0.2 mm) because of the bulk hemipelagic mud dominated deposits (Soulsby 1983). Also, skinfriction approximation is only restricted to the hemipelagic units.

The boundary layer flow speed (U_g) at 1 mab, i.e., U_{100}, was estimated from the equation of the logarithmic velocity profile that exists at the bottom few 10 m of the boundary layer of deep-sea using the following equation:

$$U(Z) = \frac{u*}{k}\left[\ln \frac{Z}{Z_0}\right] \tag{6}$$

The U_g varies logarithmically as a function of height Z above the bed and the roughness length Z_0. The values of u_* (frictional velocity; actually $u_{cr}{}^*$ at threshold) was mathematically deduced using $\mathscr{T}_{cr}$ calculated for SS size using the relation $u_{cr}{}^* = \sqrt[2]{\mathscr{T}cr/\rho}$.

Note that the current skinfriction shear stress estimated in the study holds true only for the hemipelagic sections. Skinfriction in other sand and mud turbidite sections are vogue and only estimated to compare steady current skinfriction shear stress with the turbulent stress, and hence, the value of Z_0 in those turbidite sections have not been changed to typical of coarse silt or sand.

Physical properties

Physical properties were determined onboard JOIDES Resolution during IODP Expedition 354 (Bengal Fan). We measured gamma-ray density (GRA), volume magnetic susceptibility (MS), and compressional wave velocity (Vp) with a Whole-Round Multisensor Logger. The Section Half

Imaging Logger was then used to measure color reflectance after core splitting using the LaCie color model L^*, a^*, b^* (e.g., Schanda 2007). Here, we report L^* values referring to the black-white color component (i.e., the gray value or lightness). For Site U1451A, we collected non-destructive data at 0.5–5 cm resolution and report here results for the upper 340 m core depth (measured as CSF-A), equaling roughly the last 7.5 Ma. All data were first filtered for obvious, non-sediment related outliers near the top and bottom of each section, especially in some of the silty and sandy lithologies. Details about the data are given in France-Lanord et al. (2016). The procedures to calculate and interpret physical properties are further discussed in Blum (1997) and Weber et al. (1997a).

Stratigraphy

Paleomagnetic methods are described in detail in France-Lanord et al. (2016). A more detailed description of measurements and results specific to Site U1451A can be found in Reilly et al. (2018). We used the ages of eleven reversals back to the Gilbert (5.235 Ma). All ages reported here rely on the Geomagnetic Polarity Time Scale of Gradstein et al. (2012).

Results from biostratigraphic studies used here, rely on calcareous nannofossils as well as benthic and planktonic foraminifera (France-Lanord et al. 2016). We used either the first (FO) or last occurrences (LO) depth intervals reported for a total of 15 species to provide further stratigraphic ground truth data. However, with the possibility of reworking in a partially turbiditic environment and generally large age uncertainties, we only used them for stratigraphic comparison, not as actual tie points for stratigraphic tuning.

For the younger part of Site U1451A (0–1.2 Ma), we used the detailed biomagnetostratigraphic evidence of Weber and Reilly (2018). Also, for the older part (> 7 Ma), we used the additional biostratigraphic data from Blum et al. (2018). A summary of all stratigraphic data used is shown in Fig. 3.

Stratigraphic tuning of L^*

Tuning experiments relate past variations in Earth's orbit as drivers of climate change, to the cyclic variability of responding sedimentary environment. In the Bengal Fan, long-term changes in monsoon are primarily linked to changes in orbital insolation and sea level (Kathayat et al.
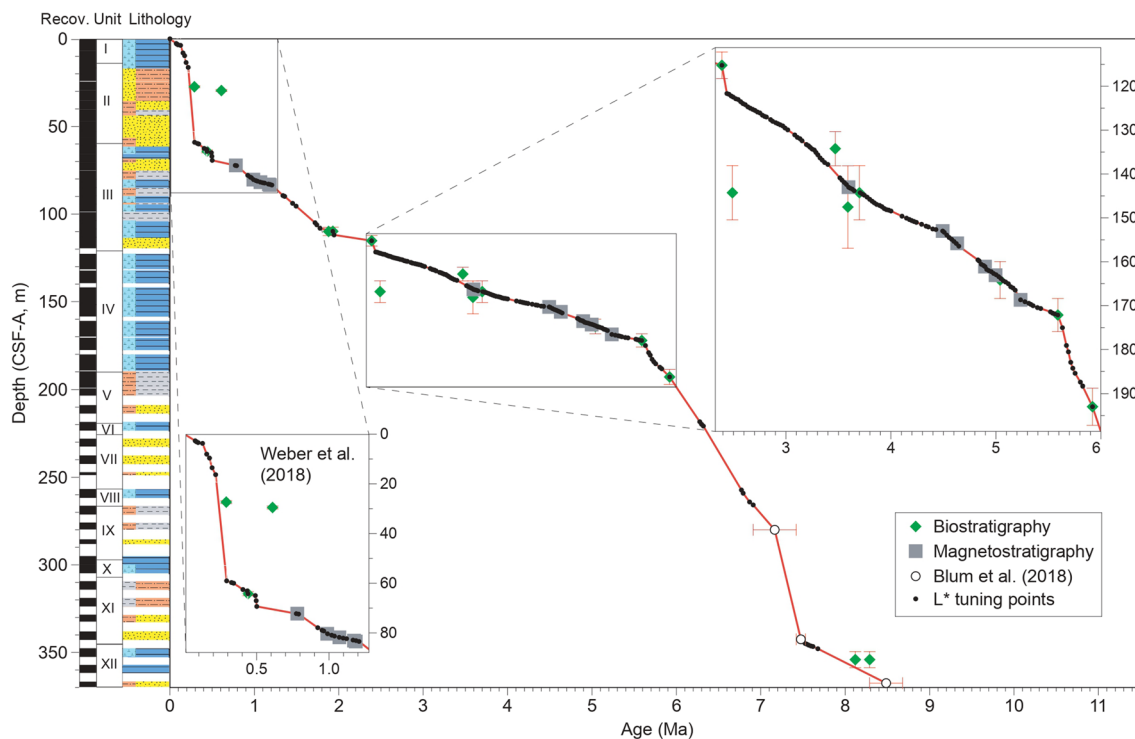

Fig. 3 Age depth model of Site U1451A. Low-resolution age control for Site U1451A is provided by magnetostratigraphy (11 reversals; gray squares) and biostratigraphy (15 datums; green diamonds with red bars indicating age uncertainties). Black dots show a total of 178 tie points employed to construct the orbital tuned, high-resolution age model. Tie points are based on tuning L^* to insolation at 20°N for the month of June using the orbital solutions of Laskar et al. (2004). Zoom-in boxes show L^* tuning of Weber and Reilly (2018) (left) and of this study (right). Additional biostratigraphic data (open circles) are from Blum et al. (2018). Lithology on the left is from France-Lanord et al. (2016)

2016; Weber et al. 2018). Tuning experiments for neighboring Site U1452 reveal a close coupling of changes in *L**, indicative of higher content of biogenic carbonate, to changes in orbital insolation over that past 200,000 years (Weber et al. 2018) in the uppermost, Late Pleistocene hemipelagic layer across the lower Bengal Fan. Also, *L** was successfully tuned to changes in the deep-sea benthic foraminifera stack of (Lisiecki and Raymo 2005) (LR04) across the entire core transect of IODP Expedition 382 revealing a second, regionally extensive, hemipelagic layer at 0.7–1.2 Ma (Weber and Reilly 2018).

Here, we conduct similar tuning experiments by correlating maxima in *L** to maxima in orbital insolation, using the software Analyseries (Paillard et al. 1996) and based on the orbital solutions provided by Laskar et al. (2004). Such tuning experiments rely on proper bio- and magnetostratigraphic control and good core recovery and only add valid information on the environmental history in continuously deposited lithologies. Accordingly, clays and calcareous clays, representing the hemipelagic component, were included while silty to sandy lithologies, representing turbiditic deposition, were excluded as far as possible. With these restrictions in mind, we mainly applied orbital tuning to a third hemipelagic layer in this study that includes core sections between ~2.4 and ~5.9 Ma (121–189 m CSF-A) (Fig. 3).

Results

Sortable silt and sediment textural records are obtained through the lithostratigraphic units I to XI (France-Lanord et al. 2016) of the Hole U1451A. Changes in major lithologies in the core are strongly reflected in the SS textural records and sediment physical properties. SS size distribution, textural parameters and physical properties are discussed below with respect to the depth and age.

SS and textural records

Lithostratigraphic units I, III, IV, VI, VIII, and X are dominated by bioturbated calcareous clay interbedded with silt and clay (France-Lanord et al. 2016). Calcareous clay lithologies represent the hemipelagic sediment in the core. The $\mathcal{SS}$ size is mostly in the domain of medium silt and varies from 14 to 27 µm in these (Fig. 4). Sand content is usually < 10 weight % and the cohesive volume percentage is high (< 50%) in calcareous clay and clay dominated sections (Fig. 4). SS volume percent is usually < 50% except in the unit IV where the SS volume percent dominates (> 50%) and cohesive volume percent decrease below 50% (Fig. 4) at the bottom of the unit (from~ 3.5 to 5.7 Ma).

The lithostratigraphic units II, V, VII, IX, and XII are dominated by silliciclastic massive sand in major with a minor amount of silt and clay. Fining upward structure and/or parallel lamination is often preserved in these lithologies, indicating these lithologies as turbidite deposits (France-Lanord et al. 2016). Petrographic observations of the fan turbidites indicate that Bengal Fan turbidites are characterized by feldspatho-quartzose to litho-feldspatho-quartzose with the plagioclase more abundant that the K-feldspar. Also, increased abundance of micas is associated with very fine sand and coarse silt lithologies (Limonta et al. 2023). The $\mathcal{SS}$ size vastly increases from medium to coarse silt range within turbidite intervals. Most high $\mathcal{SS}$ size peaks (> 31 µm; coarse silt) in these unit are associated with the medium to very thick-bedded sand turbidites. Sand contents are higher (highest 80% by weight) in sand turbidite sections, and the sand peaks are followed by a higher SS volume percentage (highest 91%, in unit II).

Threshold and current skinfriction shear stress

A criterion is set in the discussion about the selection of calcareous clay lithologies over the massive sand, silt and clay dominated one, for the estimation of shear stress matrix. However, the skinfriction is still calculated in the obvious turbidite sections, but the values do not approximate the actual shear regime. It rather helps to compare active vs. background depositional fluid shear environments. In the hemipelagic sections (i.e., calcareous clay), the skinfriction shear stress varies between 0.068 and 0.105 Pa (Pascal or Newton/m^2), and in the sand dominated section, it remarkably increases to > 0.105 Pa (Fig. 5a). Skinfriction shear stress approximation is valid in the calcareous clay lithologies and represents background shear stress regime during their deposition. The skinfriction in the sand, silt, and clay lithologies are not precise and are only kept to discriminate between the stress regime of background and active fan deposition with the boundary being at around 0.105 Newton/m^2 (Pascal). The boundary is not absolute, nor is it the same as that of the boundary between linear and turbulent flows (also usually there is a transitional state between the linear and turbulent flows in fluid dynamics). For simplicity the 0.105 Pa is considered as the boundary between active and background fan deposition to differentiate two different shear stress regimes in the BoB.

Physical properties and sediment lithology

The ability to disentangle differences in sediment lithology is critical to properly reconstruct the depositional history of the Bengal Fan. Two completely different processes determine lithology: turbiditic, and hemipelagic deposition. Using a
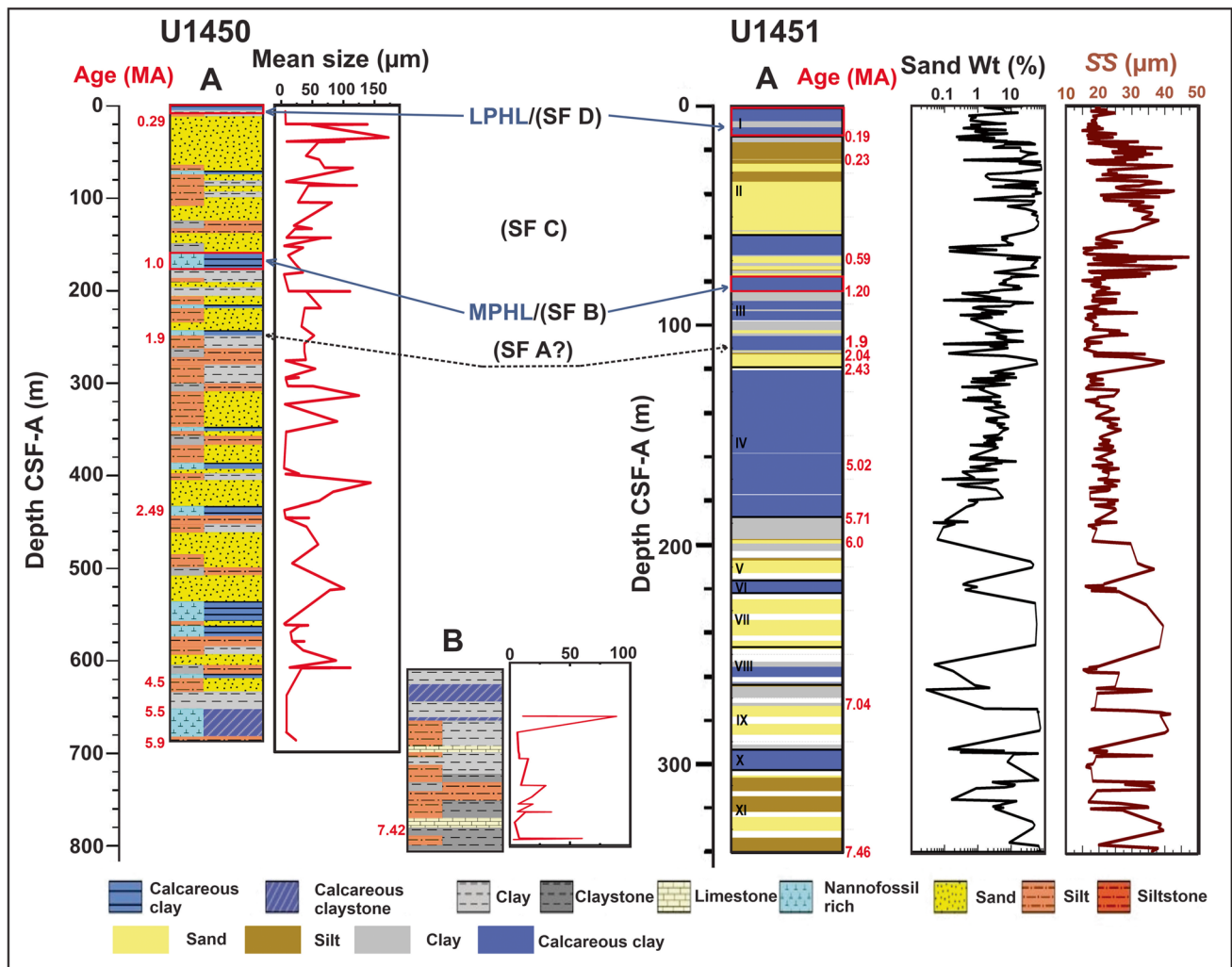
Fig. 4 Stratigraphic comparison between Site U1450 and U1451 for the last 7.5 Ma. Stratigraphy and ages at Site U1450 (hole A and B) are from France-Lanord et al. (2016). Mean grain size records of the Site U1450 are from Adhikari et al. (2018). Lithostratigraphic facies in the hole U1451A are reconstructed in the present study from high resolution sediment physical properties measured onboard JOIDES resolution. Ages are obtained from the age-depth model in the present study. (Sand wt%) and mean sortable silt (*SS*) records are shown along with the lithostratigraphic units I to XI (France-Lanord et al. 2016) and facies in the hole U1451A

novel approach (Weber and Reilly 2018), we assigned to each non-destructive measurement a simplified facies code (sand, silt, clay, calcareous clay, and volcanic ash) based on the shipboard lithologic description. This method allows for a detailed analysis of facies variability and cross correlations (Supplementary Fig. 2). Hemipelagic lithologies are fine-grained and consist primarily of calcareous clay and clay. Their physical properties show rather low GRA, MS, and Vp as well as a large variability in *L**, depending on biogenic carbonate contents. Turbiditic lithologies are coarser grained and consist dominantly of sand and silt with high GRA, MS, and Vp and darker sediment colors. Physical properties vs. U1451A lithology are depicted in Supplementary Fig. 3.

Discussion

Sedimentation history at Site U1451A from grainsize records since the late Miocene

Seismic observations along the 8°N transect (Profile GeoB97-020/027) on the lower Bengal Fan indicate that the onset of channel levee deposition started during the late Miocene and in the eastern part of the seismic profile, no other channel levee system is reported older than this (Schwenk and Spieß, 2009). The onset of channel levee deposition around 7 Ma had been reported to be concurrent with the changes in lithology from silty to muddy, decrease in overall
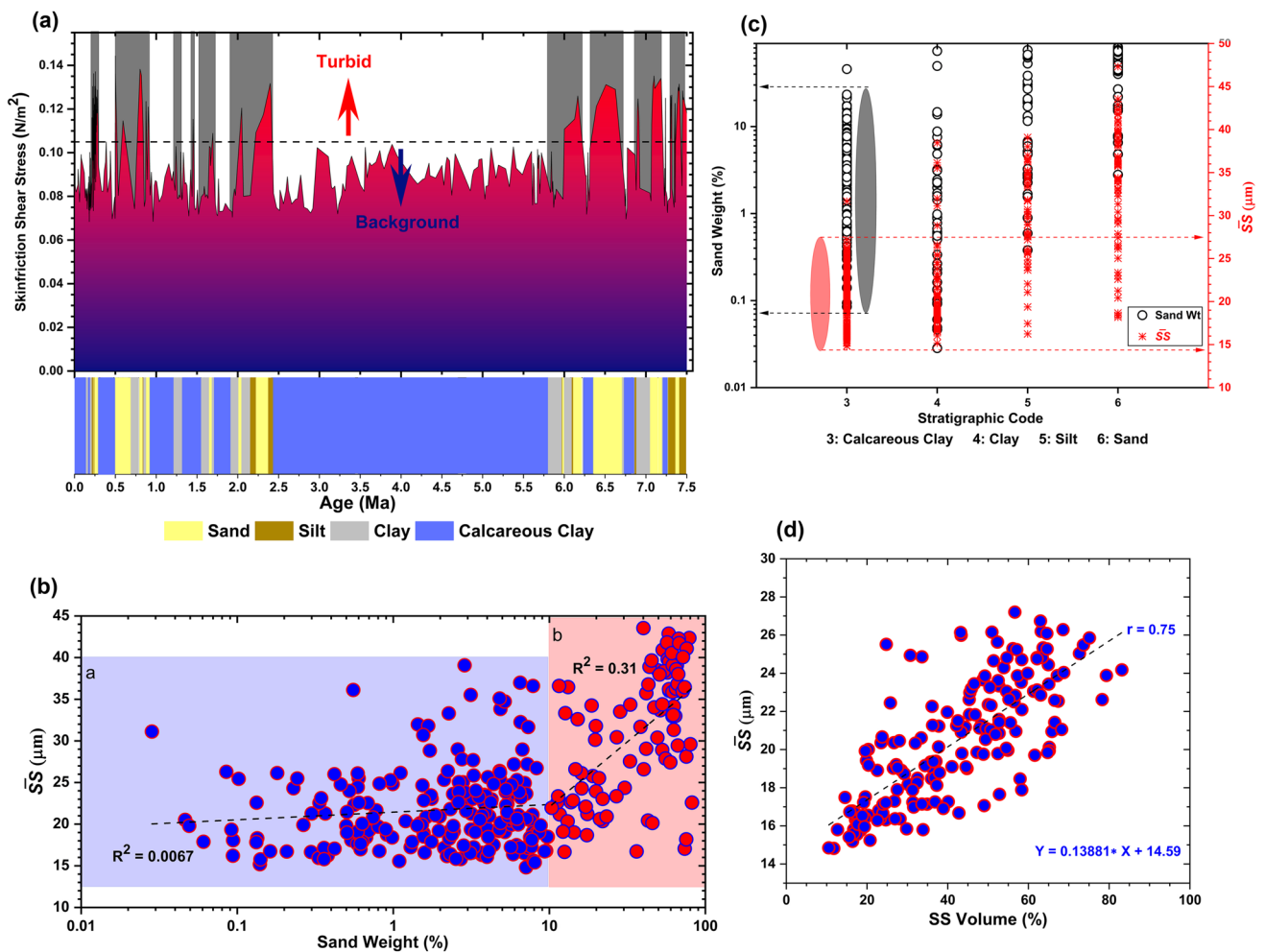
Fig. 5 **a** Skinfriction Shear stresses variation with lithology and age in the hole U1451A. Dark brown bars indicate sections of the core where skinfriction is not valid (sand, silt, and clay lithologies). **b** Sand weight percent (Sand wt%) of all the samples plotted against the mean sortable silt ($\overline{SS}$). **c** Double Y-axis plot of sand wt% and $\overline{SS}$ size vs. the lithostratigraphic code. **d** Sortable silt volume percent (SS vol%) plotted against the mean sortable silt ($\overline{SS}$). Data points all are from the hemipelagic section (calcareous clay layers) of the core

grain size, sedimentation rates, and dominance of smectite over illite (Cochran 1990; Stow et al. 1990) at ODP Leg 116 sites (Fig. 1) which were drilled along the equator and to the west of the 85° East Ridge. The late Miocene channel levee systems are argued to have been developed due to decrease in grain size within turbidity currents (Schwenk and Spieß, 2009). An assessment on the intensification or onset of the Asian monsoon during the late Miocene (An et al. 2001) was made following the sedimentological observation at ODP Leg 116 sites. Derry and France-Lanord (1996) linked the changes in Leg 116 sites lithologies to the shift in the Himalayan erosional regime from physical to chemical. However, at Site U1451A, massive sand lithologies occur between 6 and 7.4 Ma and between depths ~ 200 and ~ 340 m CSF-A (Fig. 4). The $\overline{SS}$ size in these sections are coarser (> 31 µm), and sand weight % are higher (above 60%), and the maximum grain size is 750 µm in the interval (37F-3, 130 cm;

230.22 m CSF-A) (France-Lanord et al. 2016). These massive sands may represent the late Miocene (Late Tortonian) channel levee deposition at Site U1451. The following observation depicts that the development of late Miocene channel levees systems is not linked to the overall decrease in grain size within turbidity current. Rather, the main turbidity flux was constricted between the 85° Ridge and the Ninetyeast Ridge, delivering sand to the easternmost Site (U1451A) of the 8°N transect, at the west flank of Ninetyeast Ridge, while it did not cross the 85° Ridge in the west. Also, Himalayan erosion was quite consistent (~ 1 to 2 mm yr^{-1}) since at least the Miocene, assuming that physical and chemical erosion occurred simultaneously (Lenard et al. 2020).

The sand deposits are overlain by a thick nannofossil-rich calcareous clay layer spanning nearly 4 Ma (2.4 to 5.7 Ma; Late Messinian to Early Gelasian) and a thick clay deposit at the base of unit IV at Site U1451A (Fig. 4). From

around 6 to 5.5 Ma (Late Messinian), the nannofossil-rich clay and clay appeared as major lithologies (Fig. 4), and the mean grain size was < 30 μm (Adhikari et al. 2018) at Site U1450 (8°0.42′N and 87°40.25′E at 3655 m water depth; along the central axis of the fan; see Fig. 1a). It was only after 4.5 Ma (Mid Zanclean) when sand appeared as the dominant lithology at Site U1450 which continued until around 2.4 Ma (Late Piacenzian), followed by a thin layer of nannofossil-rich calcareous clay layer possibly marking the Pliocene–Pleistocene boundary at ~ 2.5 Ma (Piacenzian-Gelasian) (Fig. 4; also see biostratigraphy of Site U1450; see France-Lanord et al. 2016). Sand continues to deposit until 1.1 Ma (Mid-late Calabrian) at Site U1450, and the mean grain size in this interval (Fig. 4) remains mostly in coarse silt to fine sand in sand rich patches (> 60 μm and as high as 140 μm; Adhikari et al. 2018). It appears that since the Late Messinian to Late Piacenzian (~ 6 to 5.5 Ma), both the sites were cut off from the active fan deposition, possibly due to deviation of active channel levee systems far westward of the Site U1450. Both the SS volume percent and $\mathcal{SS}$ size decreased during this interval of deposition at Site U1451A (Fig. 4). After the Mid Zanclean (~ 4.5 Ma), intense sand deposition took place and continued till early to middle Pleistocene boundary (at around 1.2 Ma) at the Sites U1450 (Fig. 4) while the fan deposition mostly remained distal to the easternmost part of the lower fan, and at the Hole U1451A, the hemipelagic sedimentation continued till the early Gelasian (~ 2.4 Ma). This indicates that active fan sedimentation and depocenter migrated more towards the central axis of the fan during the late Pliocene to early Pleistocene. The sedimentation rate along Profile GeoB97-020/027 (Schwenk and Spieß, 2009) is also reported to be maximum at the basin center (6.5 cm/kyr in the Pliocene) and lowest at Ninetyeast Ridge (1.5 cm/kyr in the Pliocene), thus indicating the fan sedimentation was proactive along the central axis of the fan during late Pliocene to early Pleistocene.

The Early to Middle Pleistocene (~ 2.4 to ~ 1.2 Ma) turbiditic sedimentation at Site U1451 is represented by a thin layer of massive sand and mud turbidites in the middle and at the base of unit III (Fig. 4) interlaced with calcareous clay deposits. The turbidity dominated intervals in this unit are thinner with respect to the massive sand and silty sand layer deposited at U1450 around this time. The mud turbidite layer in the middle of unit III marks the lower boundary of regionally extensive Middle Pleistocene Hemipelagic Layer (MPHL) deposited during ~ 1.2 to 0.68 Ma (Calabrian) (Weber and Reilly 2018) and traced at all Expedition 354 Sites. The MPHL believed to have been deposited concurrently with the active fan deposition (Subfan B, 1.24 to 0.68 Ma) to the west of 85° Ridge (Bergmann et al. 2020), during which no channel levee deposition took place along the 8°N transect. Thus, the turbiditic deposition prior

MPHL that is found at both Site U1450 and Hole U1451A could possibly be associated with Subfan A (1.9 to 0.96 Ma) reported by Curray et al. (2003), which was centered more towards the east of 85° Ridge and along the central axis of the fan. Thinner sand layers, high cohesive volume % (> 60%) and lower sand weight % (Fig. 4) in the samples deposited during ~ 2.4 to ~ 1.2 Ma at Site U1451 indicate that the main turbid flux and channel incision was not pervasive to the easternmost part of the lower fan along the west flanks of the Ninetyeast Ridge. However, there is a revision in the age of successive Subfan A and Subfan B as 1.2 Ma marking the base of Subfan B, which lasted until 0.68 Ma (Bergmann et al. 2020). MPHL at Site U1451 is overlain by medium-bedded to very thick bedded sand turbidites intercalated with a few successive thin to medium-bedded mud turbidite deposits. The sand turbidite beds represent intense channel incisions at the Site U1451 concomitant with the deposition of Subfan C (0.68 to 0.25 Ma; Mid-Pleistocene) all along the 8°N transect (Bergmann et al. 2020). However, sand continued to appear at the Site U1451 till ~ 0.23 Ma and peaked (> 50 wt%) around 0.23 Ma (Fig. 4). The Late Pleistocene Hemipelagic layer (LPHL) is yet another regionally extensive hemipelagic layer deposited at all Expedition 354 sites. At Hole U1451A it deposited since ~ 0.23 Ma. The LPHL at Hole U1451A is the hemipelagic deposit reciprocal to the currently active Subfan D (0.25 Ma to present) which is focused to the west of 85° Ridge (Fig. 1a, b) and include currently active channel (Weber and Reilly 2018; Bergmann et al. 2020).

Deposition flow dynamics from the Bengal Fan

SS study and calculation of shear stress matrices (current skin-friction shear tress) from $\mathcal{SS}$ size records are exclusive to the hemipelagic section in Hole U1451A. Hemipelagic deposits represent background sedimentation in the lower Bengal Fan during periods of local fan inactivity (Weber and Reilly 2018). However, background or hemipelagic sedimentation in parts of the lower fan does not necessarily mean a complete shutdown of fan deposition. It rather implies that the channelized and unchannelized turbiditic fan deposition is distal (Curray et al. 2003; Bergmann et al. 2020). Hemipelagic sediments accumulate at the lower fan at a rate of 1 to 3 cm/ka (Weber and Reilly 2018; Reilly et al. 2020), which is a magnitude higher than the typical pelagic settlement which accumulates 1 to 3 mm/ka. Thus, additional import of fine lithogenic grains and mixing with pelagic sediments is apparent. Fine lithogenic sediments from the suspension cloud of the turbid fluxes in the active fan may diffuse over larger areas and mix with pelagic drape to form hemipelagic sediments in the distal fan regions (Bergmann et al. 2020). The hemipelagic sediments in the Hole U1451A are chiefly composed of calcareous clay (France-Lanord et al. 2016).

SS records in these hemipelagic intervals exhibit sorting signatures that may arise from local deep water flow regimes associated with mixing and transporting these sediments from turbid suspension clouds in the active fan to the most distal part of the fan. The use of fine sediment record (SS record) to infer the dynamics of the depositing flows require justification whether these sediments are significantly sorted by the flow. One excellent index to distinguish the effect of sorting is given by McCave and Andrews (2019) using the degree of correlation between $\widetilde{SS}$ and the SS volume %. Grainsize records from over 30 core sites under important ocean flow regimes in high latitudes (e.g., the East and West Greenland and Labrador Currents and Nordic Sea overflows in the North, and Antarctic Circumpolar Current in the South) have been processed and argued that if fine fraction (< 63 μm) is transported and sorted, unrelated to the coarse fraction, then the correlation between $\widetilde{SS}$ and SS volume % can be used as an index to substantiate the effect of current-sorting on fine sediment irrespective of the sources of the sediments. Correlation coefficient (r) $= 0.5$ and a slope > 0.07 in $\widetilde{SS}$ vs. SS volume % are prerequisite for the SS data set to be evaluated for a valid flow intensity reconstruction. Moreover, this index is applicable to all fine grained deposits and is not only restricted to higher latitudes (McCave and Andrews 2019).

At the lower Bengal Fan, the coarse fraction is mostly sand sized siliciclastic sediment delivered through channel levee systems. In the studied core, the amount of sand (weight %) usually varies from ~10 to 82% in the turbidite sections, whereas in hemipelagic sections, it usually varies from 0 to 10% (Figs. 4 and 5). While the sand content was plotted against the varying $\widetilde{SS}$ size (Fig. 5b), different degree of associations were noticed depending on the amount of sand (> 10 wt% or < 10 wt%). When the amount of sand is $< 10\%$, it does not correlate well with the $\widetilde{SS}$ size ($R^2 = 0.004$; Fig. 5b(a)) whereas $> 10\%$ sand show certain degree of positive correlation ($R^2 = 0.31$; Fig. 5b(b)) with the $\widetilde{SS}$ size. Assignation of stratigraphic/lithological codes to the analyzed samples in the studied core showed that sand content > 10 wt% was almost always associated with the massive sand and silt lithologies in the hole U1451A (Fig. 5c). Also, the $\widetilde{SS}$ size is mostly > 27 μm in these lithologies, and the value increase with an increase in amount of sand. For these sections, the $\widetilde{SS}$ size is clearly controlled by the amount of sand (Fig. 5b(b)). Thus, changing $\widetilde{SS}$ size does not depict the vigor of bottom water flows as normally it does in contourites or sediment drift deposits. It is rather associated with the channelized and unchannelized turbid flows, which also mobilize sand-sized particles along with the SS. The SS in these sections does not represent the highest mobilizing grainsize class; thus, the skinfriction shear stress approximated from the $\widetilde{SS}$ size parameters in sections with > 10 wt% of sand does not reconstruct the shear stress

of background deep water flows, and it rather accounts for the part of turbid stress associated with turbidite deposition. On the other hand, when sand content is < 10 wt%, it does not have a conspicuous effect on the $\widetilde{SS}$ size (Fig. 5b(a)). Heavier sand sized particles do not move along with SS, and thus, SS represents the highest mobilizing grainsize class in the sections with < 10 wt% of sand. $\widetilde{SS}$ size in these sections is most possibly related to the intensity of background deep water flows that import silt and clay sized materials from the active to the most distal part of the fan. Changing $\widetilde{SS}$ size thus may support relative intensity of the deep water mass imported to the distal fan lobes.

Moreover, there is a criterion to reject $\widetilde{SS}$ size > 27 μm for the evaluation of shear stress dynamics as $\widetilde{SS}$ size > 27 is frequently associated with sand and silt lithologies in the Hole U1451A (Fig. 5c), which represent intermittent horizons reformed or deposited by turbidity currents. Calcareous clay layers, on the other hand are characterized by low sand (mostly < 10 wt%) content and $\widetilde{SS}$ size, mostly between 15 and 27 μm (Fig. 5c), therefore, best suited to the above-mentioned criteria. $\widetilde{SS}$ vs. SS volume % in the hemipelagic sections of the Hole U1451A produces an overall $r = 0.75$ and slope $= 0.13$ (Fig. 5d), which are acceptable values to regard these sediments as sorted by the local deep water flows rather than the turbidity currents. Hence $\widetilde{SS}$ size data in these sections are adopted for the approximation of the background current skinfriction shear stress.

There is a clear distinction in the shear stress regime between turbid flows and background local deep water flows in the lower Bengal Fan. Current skinfriction shear stress that is approximated in the hemipelagic section under the provision of the criteria set earlier in the discussion indicate that the hemipelagic sedimentation in the lower Bengal Fan occur at shear stress 0.068 Pa to ~0.105 Pa (Fig. 5a) delivered through local deep water masses whereas turbiditic sedimentation is associated with a shear stress > 0.105 Pa which is delivered by the turbidity currents via the channel levee systems. Hence, there are very distinct fluid shear environment present in the lower Bengal Fan during active and background fan sedimentation with shear stress boundary approximately at 0.010 to 0.0105 Pa. However, the boundary is not absolute, nor does it represent the boundary between the linear and turbulent flows (also there is transitional flow in fluid dynamics between linear and turbulent flows apparent from the Reynolds number between 500 and 2000 which largely depends on the boundary conditions). Thus the boundary at 0.105 Pa in the BoB simply differentiate two different shear stress regimes of sediment deposition in the BoB (namely active and background). Also, the current skinfriction in the Bengal Fan indicates that there are significant bottom water movements in the BoB during periods of local fan inactivity that can be related to the northern

and southern sourced deep water circulations protruding far inside the BoB.

Conclusions

We studied a deep sea Site U1451 (hole A) of IODP Expedition 354 in the lower Bengal Fan. The section from 0 to 340 m CSF-A holds the complete sedimentation record since the late Miocene, dominated by massive sand and silt lithologies and intercalated layers of clay and calcareous clay. These deposits represent active fan growth and channel levee deposition, whereas hemipelagic deposits occur in the form of calcareous clay layers at times when active fan deposition is distal to the site. High-resolution sedimentological and physical property records reveal the following:

1. Turbiditic lithologies are coarser grained and consist dominantly of sand and silt with high GRA, MS, Vp and with darker sediment colors, whereas hemipelagic lithologies are fine-grained and consist primarily of calcareous clay and clay. Their physical properties show rather low GRA, MS, and Vp as well as a large variability in $L*$ depending on biogenic carbonate contents.

2. The SS size mostly varies from 14 to 27 μm and sand content is < 10 wt% in hemipelagic lithologies. The SS size peaks (> 31 μm; coarse silt) and sand contents are higher (highest 80% by weight) in sand turbidite sections. Sand peaks are followed by a higher SS vol% > 50%.

3. Lithostratigraphy of the Sites U1450 and U1451 shows that the sand occurring at 6 to 7.4 Ma represents the late Miocene channel levee deposition at Site U1451. The hemipelagic layer deposited during 2.4 to 5.7 Ma indicates that the easternmost part of lower fan was completely shut down to active fan deposition. Concurrent to Subfan A, thin and massive sand layers appeared at Site U1451 and U1450, respectively. Subfan B is manifested by regionally extensive MPHL at all 354 sites, followed by channel levee deposition during Subfan C, followed by yet another hemipelagic layer (LPHL) deposited during currently active Subfan D, thus indicating a complex history of channel levee migration and depocenter shifts across fan margins.

4. Sand < 10 wt% does not have an effect on SS size distribution whereas SS size is mostly affected when sand > 10 wt%. Thus, SS size data in sand and lithologies are not suited for calculation of shear stress matrices. Also, SS size > 27 μm was rejected because it is associated with turbidite layers. In hemipelagic sections, on the other hand, SS size is < 27 μm and sand < 10 wt%. Also SS vs.

SS vol% produces an overall $r = 0.75$ and slope = 0.13 which substantiate the effect of current-sorting.

5. SS size data in hemipelagic layers are adopted for the approximation of the background current skinfriction shear stress. A distinct shear stress regime exists between turbid flows and background local deep water flows in the lower Bengal Fan, i.e., 0.068 Pa to ~ 0.105 Pa during hemipelagic sedimentation whereas > 0.105 Pa during the turbidity deposits with the boundary being at 0.010 to 0.0105 Pa.

Declarations

Ethics approval I agree with the ethics approval in all our papers.

Consent to participate We agree to participate.

Consent for publication I agree to the publication including appropriate statements.

Competing interests The authors declare no competing interests.

References

Adhikari SK, Sakai T, Yoshida K (2018) Data report: grain size analysis of Bengal Fan sediments at Sites U1450 and U1451, IODP Expedition 354. In France-Lanord C, Spiess V, Klaus A, Schwenk T and the Expedition 354 Scientists, Bengal Fan. Proc Int Ocean Discovery Prog 354: College Station, TX (International Ocean Discovery Program). https://doi.org/10.14379/iodp.proc.354.202.2018

Alam M, Alam MM, Curray JR, Chowdhury MLR, Gani MR (2003) An overview of sedimentary geology of the Bengal basin in relation to the regional framework and basin-fill history. Sediment Geol 155:179–208

An Z, Kutzbach JE, Prell WL, Porter SC (2001) Evolution of Asian monsoons and phased uplift of the Himalaya-Tibetan plateau since late Miocene times. Nature 411:62–66

Bergmann F, Schwenk T, Spiess V, France-Lanord C (2020) Middle to Late Pleistocene architecture and stratigraphy of the lower Bengal Fan—Integrating multichannel seismic data and IODP Expedition 354 results. Geochem Geophys Geosyst 21:e2019GC008702. https://doi.org/10.1029/2019GC008702

Bertram CJ, Elderfield H (1993) The geochemical balance of the rare-earth elements and neodymium isotopes in the oceans. Geochem Cosmochim Act 57:1957–1986

Bianchi GG, McCave IN (1999) Holocene periodicity in North Atlantic climate and deep-ocean flow south of Iceland. Nature 397:516

Blott SJ, Pye K (2001) GRADISTAT: a grain size distribution and statistics package for the analysis of unconsolidated sediments. Earth Surf Processes Landf 26:1237–1248

Blum M, Rogers K, Gleason J, Najma Y, Cruz J, Fox L (2018) Allogenic and autogenic signals in the stratigraphic record of the deep-sea Bengal Fan. Sci Rep 8:7973

Blum P (1997) Physical properties handbook: a guide to the shipboard measurement of physical properties of deep-sea cores. Technical Note 26, Ocean Drilling Program, College Station, Texas

Cochran JR (1990) Himalayan uplift, sea level, and the record of Bengal Fan sedimentation at the ODP Leg 116 sites. In J.R. Cochran, D.A.V. Stow, et al., Proc ODP, Scientific Results, 116, College Station, TX (Ocean Drilling Program): 397-414. https://doi.org/10.2973/odp.proc.sr.116.144.1990

Curray JR, Moore DG (1971) Growth of the Bengal deep-sea fan and denudation in the Himalayas. Geol Soc Am Bull 82:563–572

Curray JR, Emmel FJ, Moore DG (2003) The Bengal Fan: morphology, geometry, stratigraphy, history and processes. Mar Pet Geol 19(10):1191–1223. https://doi.org/10.1016/S0264-8172(03)00035-7

Derry LA, France-Lanord C (1996) Neogene Himalayan weathering history and river [87]Sr/[86]Sr: impact on the marine Sr record. Earth Planet Sci Let 142:59–74

Derry L, France-Lanord C (1997) Himalayan weathering and erosion fluxes: climate and tectonic controls. In: Ruddiman W (ed) Tectonic uplift and climate change. Springer, US, pp 289–312

France-Lanord C, Spiess V, Klaus A, Schwenk T, Expedition 354 Scientists (2016) Bengal Fan. Proc Internat Ocean Discovery Program 354, College Station, TX (International Ocean Discovery Program). https://doi.org/10.14379/iodp.proc.354.105.2016

Gordon AL, Giulivi CF, Takahashi T, Sutherland S, Morrison J, Olson D (2002) Bay of Bengal nutrient-rich benthic layer. Deep Sea Res II 49(7–8):1411–1421. https://doi.org/10.1016/S0967-0645(01)00161-8

Goswami V, Singh SK, Bhushan R (2014) Impact of water mass mixing and dust deposition on Nd concentration and εNd of the Arabian Sea water column. Geochem Cosmochim Act 145:30–49

Gradstein FM, Ogg JG, Schmitz MD, Ogg GM (2012) The geologic time scale. Elsevier, Amsterdam

Hall IR, Bianchi GG, Evans JR (2004) Centennial to millennial scale Holocene climatedeep water linkage in the North Atlantic. Quat Sci Rev 23:1529–1536

Jessen SP, Rasmussen TL (2015) Sortable silt cycles in Svalbard slope sediments 74–0 ka. J Quat Sci 30:743–753

Kathayat G, Cheng H, Sinha A, Spötl C, Edwards RL, Zhang H, Li X, Yi L, Ning Y, Cai Y, Lui WL, Breitenbach SFM (2016) Indian monsoon variability on millennial-orbital timescales. Sci Rep 6:24374

Kawsar M, Manoj MC, Weber ME (2022) Reconstructing dynamics of Northern and Southern sourced bottom waters sortable silt records in the lower Bengal Fan during last 200 ka. J Appl Reg Geol. https://doi.org/10.1127/zdgg/2022/0318

Kumar MD, Li YH (1996) Spreading of water masses and regeneration of silica and Ra-226 in the Indian Ocean. Deep-Sea Res II 43:83–110

Laskar J, Robutel P, Joutel F, Gastineau M, Correia ACM, Levrard B (2004) A long-term numerical solution for the insolation quantities of the Earth. Astron Astrophys 428:261–285

Lathika N, Rahaman W, Tarique M, Gandhi N, Kumar A, Thamban M (2021) Deep water circulation in the Arabian Sea during the last glacial cycle: implications for paleo-redox condition, carbon sink and atmospheric CO_2 variability. Quat Sci Rev 257:106853. https://doi.org/10.1016/j.quascirev.2021.106853

Lenard SJP, Cruz J, France-Lanord C, Lavé J, Reilly BT (2020) Data report: calcareous nannofossils and lithologic constraints on the age model of IODP Site U1450, Expedi- tion 354, Bengal Fan. In France-Lanord ., Spiess V, Klaus A, Schwenk T, and the Expedition 354 Scientists, Bengal Fan. Proc Internat Ocean Discovery Program 354. College Station, TX (International Ocean Discovery Program). https://doi.org/10.14379/iodp.proc.354.203.2020 .

Li N, Yang X, Peng J, Zhou Q, Su Z (2019) Deep-water bottom current evolution in the northern South China Sea during the last 150 kyr: evidence from sortable-silt grain size and sedimentary magnetic fabric. J Asian Earth Sci 171:78–87. https://doi.org/10.1016/j.jseaes.2017.06.005

Limonta M, Garzanti E, Resentini A (2023) Petrology of Bengal Fan turbidites (IODP Expeditions 353 and 354): provenance versus diagenetic control. J Sediment Res 93(4):256–272. https://doi.org/10.2110/jsr.2022.071

Lisiecki LE, Raymo ME (2005) A Pliocene-Pleistocene stack of 57 globally distributed benthic $\delta^{18}O$ records. Paleoceanography 20:PA1003. https://doi.org/10.1029/2004PA001071

McCave IN, Andrews JT (2019) Distinguishing current effects in sediments delivered to the ocean by ice. I. Principles, methods and examples. Quat Sci Rev 212:92–107

McCave IN, Manighetti B, Robinson SG (1995) Sortable silt and fine sediment size/composition slicing: Parameters for palaeocurrent speed and palaeoceanography. Palaeoceanography 10(3):593–610

McCave IN, Kiefer T, Thornalley DJR, Elderfield H (2005) Deep flow in the Madagascar– Mascarene Basin over the last 150000 years. Philos Trans R Soc A 363:81–99

McCave IN, Thornalley DJR, Hall IR (2017) Relation of sortable silt grain-size to deep-sea current speeds: calibration of the 'Mud Current Meter.' Deep Sea Res I 127:1–12

McCave IN (2008) Size sorting during transport and deposition of fine sediments: sortable silt and flow speed. In: Contourites (Eds. Rebesco M, Camerlenghi A), Dev Sedimentol 60:121–142. https://doi.org/10.1016/S0070-4571(08)10008-5

Paillard D, Labeyrie L, Yiou P (1996) Macintosh Program performs time-series analysis. EOS Transactions 77:379–379

Piotrowski AM, Banakar VK, Scrivner AE, Elderfield H, Galy A, Dennis A (2009) Indian Ocean circulation and productivity during the last glacial cycle. Earth Planet Sci Lett 285:179–189

Praetorius SK, McManus JF, Oppo DW, Curry WB (2008) Episodic reductions in bottom-water currents since the last ice age. Nat Geosci 1:449–452. https://doi.org/10.1038/ngeo227

Rao DP, Murty VSN (1992) Circulation and geostrophic transport in the Bay of Bengal. Physical process in the Indian seas. Proc First Conv, ISPSO 1990:79–85

Reilly BT, Stoner JS, Selkin P, Savian J, Meynadier L (2018) Data report: paleomagnetic directions from IODP Expedition 354, Hole U1451A, Cores 23H and 24H. In: Spiess V, Klaus A, Schwenk T, Scientists E (eds) France-Lanord C. Bengal Fan. Proc Internat Ocean Discovery Program. College Station, TX

Reilly BT, Bergmann F, Weber ME, Stoner JS, Selkin P, Meynadier L et al (2020) Middle to late Pleistocene evolution of the Bengal Fan: integrating core and seismic observations for chronostratigraphic modeling of the IODP Expedition 354, 8° north transect. Geochem Geophys Geosyst 21:e2019GC008878. https://doi.org/10.1029/2019GC008878

Roberts AP, Chiang L, Heslop D, Florindo F, Larrasoana JC (2012) Searching for single domain magnetite in the '"pseudo-singledomain"' sedimentary haystack: Implications of biogenic magnetite preservation for sediment magnetism and relative paleointensity determinations. J Geophys Res 117:B08104. https://doi.org/10.1029/2012JB009412

Sastry JS, Rao DP, Murty VSN, Sarma YVB, Suryanarayana A, Babu MT (1985) Water mass structure in the Bay of Bengal. Mahasagar-Bull Natl Inst Ocean 18:153–162

Schanda J (2007) CIE Colorimetry, Colorimetry. John Wiley & Sons, Inc., 25–78. https://doi.org/10.1002/9780470175637.ch3

Schwenk T, Spieß V (2009) Architecture and stratigraphy of the Bengal Fan as response to tectonic and climate revealed from high-resolution seismic data. External Controls on Deep-Water Depositional Systems. Special Publication-SEPM 92:107–131

Schwenk T, Spieß V, Hübscher C, Breitzke M (2003) Frequent channel avulsions within the active channel–levee system of the middle Bengal Fan—an exceptional channel–levee development derived from Parasound and Hydrosweep data. Deep Sea Res Part II 50(5):1023–1045. https://doi.org/10.1016/S0967-0645(02)00618-5

Schwenk T, Spieß V, Breitzke M, Hübscher C (2005) The architecture and evolution of the Middle Bengal Fan in vicinity of the active channel–levee system imaged by high-resolution seismic data. Mar Petrol Geol 22(5):637–656. https://doi.org/10.1016/j.marpetgeo.2005.01.007

Shankar D, Vinayachandran PN, Unnikrishnan AS (2002) The monsoon currents in the north Indian Ocean. Prog Oceanogr 52(1):63–120. https://doi.org/10.1016/S0079-6611(02)00024-1

Shields A (1936) Application of similarity principles, and turbulence research to bed-load movement. California Institute of Technology, Pasadena (translate from German)

Singh SP, Singh SK, Goswami V, Bhushan R, Rai VK (2012) Spatial distribution of dissolved neodymium and εNd in the Bay of Bengal: role of particulate matter and mixing of watermasses. Geochim Cosmochim Act 94:38–56. https://doi.org/10.1016/j.gca.2012.07.017

Soulsby R L, Whitehouse RJS, (1997) Threshold of sediment motion in coastal environments. In: Pacific Coasts and Ports '97: Proceedings of the 13th Australasian Coastal and Ocean Engineering Conference and the 6th Australasian Port and Harbour Conference. Christchurch, NZ: Centre for Advanced Engineering, University of Canterbury 1:145–150

Soulsby RL, (1983) The bottom boundary layer in shelf seas. B. Johns (Ed.), Physical oceanography of coastal and shelf seas, Elsevier Oceanography Series, Amsterdam 35:189–266. https://doi.org/10.1016/S0422-9894(08)70503-8

Spieß V, Hübscher C, Breitzke M, Böke W, Krell A, von Larcher T et al, (1998) Report and preliminary results of R/V Sonne cruise 125, Cochin–Chittagong, 17.10.-17.11.97: Ber Fachber Geowiss, Univ Bremen 123. http://elib.suub.uni-bremen.de/ip/docs/00010242.pdf

Stow DA, Amano K, Batson B, Brass GW, Corrigan J, Raman C et al (1990) Sediment facies and processes on the distal Bengal Fan, Leg 116 Cochran JR, Stow DAV et al. Proc Ocean Drilling Project Leg 116:377–396

Thornalley DJR, Oppo DW, Ortega P, Robson JI, Brierley CM, Davis R, Hall IR, Moffa-Sanchez P, Rose NL, Spooner PT, Yashayaev IM, Keigwin LD (2019) Anomalously weak Labrador Sea convection and Atlantic overturning during the past 150 years. Nature 556(7700):227–230. https://doi.org/10.1038/s41586-018-0007-4

Weber ME, Reilly BT (2018) Hemipelagic and turbiditic deposits constrain lower Bengal Fan depositional history through Pleistocene climate, monsoon, and sea level transitions. Quat Sci Rev 199:159–173

Weber ME, Niessen F, Kuhn G, Wiedicke M (1997) Calibration and application of marine sedimentary physical properties using a multi-sensor core logger. Mar Geol 136:151–172

Weber ME, Wiedicke MH, Kudrass HR, Hübscher C, Erlenkeuser H (1997) Active growth of the Bengal Fan during sea-level rise and highstand. Geology 25:315–318

Weber ME, Wiedicke-Hombach M, Kudrass HR, Erlenkeuser H (2003) Bengal Fan sediment transport activity and response to climate forcing inferred from sediment physical properties. Sediment Geol 155:361–381

Weber ME, Lantzsch H, Dekens P, Das SK, Reilly BT, Martos YM, Meyer-Jacob C, Agrahari S, Ekblad A, Titschack J, Holmes B, Wolfgramm P (2018) 200,000 years of monsoonal history recorded on the lower Bengal Fan - strong response to insolation forcing. Global Planet Change 166:107–119. https://doi.org/10.1016/j.gloplacha.2018.04.003

Wyrtki K (1973) An equatorial jet in the Indian Ocean. Science 181:262–264

You YZ (2000) Implications of the deep circulation and ventilation of the Indian Ocean on the renewal mechanism of North Atlantic Deep Water. J Geophys Res 105:23895–23926

Zhisheng A, Kutzbach JE, Prell WL, Porter SC (2001) Evolution of Asian monsoons and phased uplift of the Himalaya-Tibetan plateau since Late Miocene times. Nature 411(6833):62